Transmission of persistent ionizing radiation-induced foci through cell division in human primary cells

Aurelie Vaurijoux, Pascale Voisin, Amélie Freneau, Joan Francesc Barquinero, Gaetan Gruel

Transmission of persistent ionizing radiation-induced foci through cell division in human primary cells

Aurelie Vaurijoux[1], Pascale Voisin[1], Amelie Freneau[1], Joan Francesc Barquinero[2] and Gaetan Gruel[1]

[1] Institut de Radioprotection et de Sureté Nucléaire (IRSN), Laboratoire de Dosimétrie Biologique, BP 17, 92262 Fontenay aux roses cedex, France.

[2] Universitat Autònoma de Barcelona, Faculty of Biosciences, 08193 Cerdanyola del Vallès, Spain.

Corresponding author:
Aurelie Vaurijoux
Institut de Radioprotection et de Sureté Nucléaire (IRSN),
Laboratoire de Dosimétrie Biologique (PRP-HOM/SRBE/LDB),
BP 17, 92262 Fontenay aux roses cedex, France.
Telephone number: +33 1 58 35 92 64
Fax number: +33 1 58 35 84 67
Email: aurelie.vaurijoux@irsn.fr

Abstract

Unrepaired DNA double-strand breaks (DSBs) induced by ionizing radiation are associated with lethal effects and genomic instability. After the initial breaks and chromatin destabilization, a set of post-translational modifications of histones occurs, including phosphorylation of serine 139 of histone H2AX (γH2AX), which leads to the formation of ionizing radiation-induced foci (IRIF). DSB repair results in the disappearance of most IRIF within hours after exposure, although some remain 24 hours after irradiation. Their relation to unrepaired DSBs is generally accepted but still controversial. This study evaluates the frequency and kinetics of persistent IRIF and analyzes their impact on cell proliferation. We observed persistent IRIF up to 7 days postirradiation, and more than 70% of cells exposed to 5 Gy had at least one of these persistent IRIF 24 hours after exposure. Moreover we demonstrated that persistent IRIF did not block cell proliferation definitively. The frequency of IRIF was lower in daughter cells, due to asymmetric distribution of IRIF between some of them. We report a positive association between the presence of IRIF and the likelihood of DNA missegregation. Hence, the structure formed after the passage of a persistent IRI focus across the S and G2 phases may impede the correct segregation of the affected chromosome's sister chromatids. The ensuing abnormal resolution of anaphase might therefore cause the nature of IRIF in daughter-cell nuclei to differ before and after the first cell division. The resulting atypical chromosomal assembly may be lethal or result in a gene dosage imbalance and possibly enhanced genomic instability, in particular in the daughter cells.

Keywords:

Ionizing radiation, γH2AX foci, cell division, chromosome break, DNA double strand break.

1. Introduction

DNA damage is a key event in cell response to ionizing radiation, one involving genetic and epigenetic modifications that may affect the homeostasis of healthy tissues in exposed individuals. In particular, DNA double-strand breaks (DSBs) that are incorrectly or not repaired are associated with lethal effects and genomic instability [1]. DSBs trigger activation of phosphatidylinositol-3'-OH kinase-related kinases (PIKK), such as ataxia telangiectasia mutated (ATM) and DNA-dependent protein kinase (DNA-PK); these, in turn, phosphorylate the histones H2AX located around the break, at serine 139 [2–5]. This phosphorylation of H2AX (γH2AX) quickly spreads over several megabases on the adjacent chromatin [5,6] and results in the formation of microscopically visible nuclear foci, known as ionizing radiation-induced foci (IRIF). One explanation for this extensive phosphorylation postulates that DSBs cause massive relaxation of chromatin coiling [6]. γH2AX initiates the formation of a platform to attract and retain proteins, such as Nijmegen breakage syndrome 1 (NBS1), mediator of DNA damage checkpoint protein 1 (MDC1), breast cancer susceptibility 1 (BRCA1), and p53-binding protein 1 (53BP1); these lead in turn to the recruitment of DNA damage repair proteins [7–10].

The number of γH2AX IRIF peaks at 30 minutes after exposure, and most of these IRIF disappear within hours of exposure [5,6]. This disappearance is thought to be related to DSB repair and restoration of chromatin integrity and structure [11,12]. However, some IRIF remain 24 hours after exposure [13], and their association with residual DSBs is generally accepted since DDR proteins are still present within these persistent IRIF [13,14]. Although the nature, role, and consequences of these IRIF are still unclear, some studies suggest that they are involved in the inhibition of G1/S progression [13] but also in radiation-induced cellular senescence and death [15,16].

In this work, we evaluated the kinetics of the appearance and disappearance of γH2AX and 53BP1 IRIF. We characterized persistent IRIF up to 7 days after exposure to ionizing radiation and evaluated their impact on the resumption of the cell cycle and the division of normal human primary cells irradiated during the G0/G1 phase.

2. Materials and Methods

2.1. Cell cultures and irradiation

Primary human umbilical vein endothelial cells (HUVECs, C2519A, lot. 0000087758) were isolated by Lonza from human tissue (from 3 females and 1 male) donated after permission was obtained for its use in research applications by informed consent or legal authorization. All cells tested negative for mycoplasma, bacteria, yeast, and fungi. Cell lots and donors were tested and negative for HIV-1, hepatitis B, and hepatitis C. The HUVECs were cultured at 37 °C, with 95% humidity and 5% CO_2 in EGM-2 media optimized for the proliferation of endothelial cells and supplemented with 5% fetal bovine serum, hydrocortisone, hFGF-B, VEGF, R3-IGF-1, ascorbic acid, hEGF, gentamicin, and amphotericin-B (EGM-2MV BulletKit, CC-3202, Lonza). We used HUVEC primary cells at low passages and evaluated their

cytogenetic status by M-FISH during passages 2 (P2) and 4 (P4) [17]. No clonal abnormality was observed, and the proportions of males and females obtained by cytogenetic analysis were consistent with the initial cell pools (3 females and 1 male). To obtain cells in G0/G1 phase of the cell cycle at irradiation, we synchronized cells by contact inhibition induced in confluent culture. Subsequently, synchronized cells were seeded on glass in Nunc® Lab-Tek® II chamber slide systems (Thermo Fisher Scientific) for 5 hours before irradiation. The experimental protocol was designed to ensure that the DNA damage took place in cells in G0/G1 (initial synchronization of the cells) but also that nothing other than irradiation could block resumption of the cell cycle. We therefore verified that at 5 hours post-seeding, cells were in G0/G1 and almost all adherent and that the density of seeding would allow future cell growth. An Elekta Synergy Platform (linac accelerator) was used to deliver X-rays with a maximum energy of 4 MeV (4 MVp) at a dose rate of 2.3 $Gy \cdot min^{-1}$ and with a delivered dose uncertainty rate of 7%. We delivered two different doses: 1 and 5 Gy. Culture media were not renewed after irradiation. To monitor cell proliferation we added 50 µM 5-bromo-2'deoxyuridine (BrdU; B-5002, Sigma-Aldrich) to the cell culture medium just after its exposure to X-rays.

2.2. Immunofluorescence staining

Cells were washed with 1X PBS (14190-094, Life Technologies), fixed with 4% paraformaldehyde solution (199431LT, Affymetrix), and permeabilized with 0.5% Triton X-100 (T8787, Sigma-Aldrich). The following primary antibodies were used in this study: mouse IgG1 monoclonal anti-phospho-histone H2AX (Ser139) antibody (dilution of 1/800; 05-636, clone JBW301, Upstate), rabbit IgG polyclonal anti-53BP1 antibody (dilution of 1/1000; A300-272A, Bethyl Laboratories), and rat IgG2a monoclonal anti-BrdU antibody (dilution of 1/200; ab6326, clone BU1/75 (ICR1), Abcam). Antibodies were diluted in 1X PBS with 2% (w/v) BSA (bovine serum albumin; A9418, Sigma-Aldrich) and incubated with cells for 1 hour at room temperature (RT). After washing, the following secondary antibodies were used: donkey anti-mouse IgG polyclonal antibody conjugated to FITC (1 $mg.ml^{-1}$; dilution of 1/100; AP192F, Chemicon), donkey anti-rat IgG polyclonal conjugated to Alexa Fluor® 594 (2 $mg.ml^{-1}$; dilution of 1/500; A21209, Life Technologies), and goat anti-rabbit IgG polyclonal conjugated to Alexa Fluor® 647 (2 $mg.ml^{-1}$; dilution of 1/1000; A21245, Life Technologies) or chicken anti-goat IgY polyclonal conjugated to Alexa Fluor® 647 (2 $mg.ml^{-1}$, dilution of 1/500; A21469, Life Technologies). They were diluted in PBS with 2% BSA and incubated with cells for 1 hour at RT. DNA was stained with DAPI (0.2 $\mu g.ml^{-1}$; 1050A, Euromedex) and mounted with ProLong® Antifade Reagents (P36930, Life Technologies). For BrdU labeling, we performed a DNA denaturation step between fixation and permeabilization by incubation for 30 minutes at RT in 1 M HCL (Prolabo).

2.3. Analysis of binucleated cells

To obtain binucleated cells, cytokinesis was blocked with cytochalasin B (0.35 µg.ml^{-1}; c2743, Sigma-Aldrich) and added to culture medium 24 hours after exposure to 5-Gy irradiation. *In situ* immunofluorescence staining was performed 24 hours after cytochalasin B treatment began.

2.4. Image acquisition and analysis

Images were acquired and analyzed with the Scan^R platform (Olympus), as described previously [17]. Briefly, images were acquired on an inverted Olympus IX81 fluorescence microscope with a UPLSAPO 100XO oil immersion objective (Olympus) and an NA of 1.4; the microscope was coupled with an Orca R² CCD camera (Hamamatsu) and a motorized SCAN IM IX2 stage (Märzhäuser). Image analysis was performed with Scan^R analysis software (Olympus). An edge segmentation algorithm based on Canny's method [18] was used to detect nuclei in the DAPI channel (main object) and γH2AX foci in the FITC channel (sub-object 1). A first selection based on the area and circularity of the nuclei excluded clusters of cells and cellular debris. Cells were selected in the different phases of the cell cycle by assessing the integrated intensity of the DAPI signal (DNA content) combined with the integrated intensity of the γH2AX signal in the entire nucleus, which increased dramatically increased in S phase [17,19].

3. Results

3.1. Characterization of IRIF as a function of time and dose

To investigate the IRIF dynamics induced in G0/G1 phase, we exposed synchronized G0/G1 phase human umbilical vein endothelial cells (HUVECs) to 1 or 5 Gy of 4 MV X-rays and studied IRIF from 10 minutes to 7 days after exposure by monitoring γH2AX foci. Using automated detection of nuclei and foci, we analyzed a mean of 4,000 cells for each condition so that we could screen subpopulations of cells or foci by different characteristics, such as size, shape, or cell-cycle phase, and weight their representativeness within the entire population of exposed cells. All results presented here concern only cells in the G0/G1 phase of the cell cycle.

The number of γH2AX IRIF peaked 30 minutes after exposure (Fig. 1A), consistent with previous reports [5,6,20]. By 24 hours after exposure, the frequency of γH2AX IRIF per nucleus decreased by more than 90% for both doses. Some IRIF nonetheless remained observable, their numbers dose-dependent; we observed 4.6 times more IRIF for the cells exposed to 5 Gy compared with 1 Gy of irradiation: 4.2 ± 0.5 and 0.9 ± 0.2 γH2AX IRIF per nucleus, respectively (Table 1). By 7 days after exposure to 5 Gy, the mean number of γH2AX IRIF per nucleus was still 0.8 ± 0.3, still significantly more than that measured in unirradiated cells (0.4 ± 0.2 per nucleus; Table 1). Co-immunostaining of γH2AX and 53BP1 showed nearly invariable co-location between these proteins from 10 minutes to 7 days after exposure (Fig. 2C).

To characterize these γH2AX/53BP1 IRIF over time, we measured the area of about 100,000 to 460,000 early IRIF (before 24 hours postexposure) and 9,600 to 22,000 persistent IRIF (from 24 hours postexposure). Their area increased as their number per nucleus decreased (Fig. 1). Most early IRIF were

small, whereas persistent IRIF were characterized by their larger size (Fig. 1B), in accordance with previous work [13]. Comparison of the distributions of IRIF areas at 30 minutes and 72 hours confirmed this observation. Fig. 2 depicts the two different ranges of size observed for early (Fig. 2A) and persistent (Fig. 2B) IRIF induced specifically by ionizing radiation (i.e., normalized with respect to the corresponding non-irradiated condition). Hence, early IRIF were characterized by an area ranging from 0.2 to 1.3 μm^2 (Fig. 2A) and persistent IRIF by an area greater than 1.1 μm^2 (Fig. 2B). We therefore use these areas as thresholds to study persistent IRIF in the rest of this work and report in Table 1 the frequencies of these IRIF as a function of time since irradiation and dose. A basal rate of foci with size characteristics similar to the persistent IRIF was observed in non-irradiated cells.

At 24 hours after exposure, 12.7% ± 3.3% of the cells exposed to 1 Gy irradiation contained at least one persistent IRI focus (Fig. 3), that is, about one fifth of the percentage among 5 Gy irradiated cells: 73.2% ± 12.8%. These results underline the substantial number of cells affected, especially as only 4.3% ± 0.01% of non-irradiated cells contained at least one large γH2AX focus.

3.2. Persistent IRIF and cell proliferation

We investigated the role of the cell cycle in IRIF behavior. To identify the cells that had completed a full cell cycle, we added BrdU just after irradiation. Fig. 4A and 4B show the cell distribution at different phases of the cell cycle as a function of dose and time. The results for unirradiated cells were consistent with normal HUVEC cell growth in our cell culture conditions. At 24 hours after exposure, the cell cycle had resumed, dose-dependently (Fig. 4A). Consistent with the cell synchronization in the G0/G1 phase at irradiation, the main activated checkpoint was G1/S. The lack of any significant increase in the proportion of cells in G2 at 24 (Fig. 4A) or 48 hours (Fig. 4B) after irradiation suggests that the G2/M checkpoint was not significantly activated in our experimental conditions.

The density of the cell monolayer (Fig. 4C) was consistent with cell cycle resumption between 24 and 48 hours after irradiation. Interestingly, although BrdU-positive cells in G0/G1 accounted for almost half of the cell population exposed to 5 Gy (Fig. 4B), monolayer density did not increase significantly (Fig. 4C). Phase contrast live-cell imaging of synchronized cells exposed to 5 Gy showed that around 45% of cells that reached M phase (when the adherent cells became transiently spherical) died. Of the 157 cells that entered M phase, 86 produced adherent daughter cells, while the other 71 died during this phase. This finding may explain the apparent stability of the cell monolayer density after irradiation with 5 Gy, despite the presence of dividing cells.

At 24 hours after exposure, most of the cells with persistent γH2AX/53BP1 IRIF were halted in G0/G1, that is, were still BrdU-negative (Fig. 5A). Surprisingly, the situation was reversed at 48 hours: as most of the cells with persistent γH2AX/53BP1 IRIF were G0/G1 BrdU-positive (16.7%±1.3% and 42.3%±3.6% for 1 and 5 Gy, respectively, see Fig. 5A and B). These results indicate that the presence of persistent IRIF does not permanently prevent cells from progressing through the cell cycle. It is interesting to note that

BrdU incorporation significantly increased the frequency of large foci measured in unirradiated cells after cell division; at 48 hours, their frequency of cells with large foci was close to that measured for cells exposed to a 1-Gy dose (Fig 5A). To prevent this from interfering with subsequent measurements, we focused on cells exposed to the 5 Gy dose.

3.3. Transmission of persistent IRIF to daughter cells

To investigate the transmission of persistent IRIF through cell division, we determined its frequency as a function of BrdU labeling and time since exposure. The frequency of persistent IRIF decreased significantly between 24 and 48 hours after exposure, apparently simultaneously with the resumption of cell cycle progression (Figs. 4, 5, and 6A). Interestingly, the frequency of persistent IRIF remained stable over time in each subpopulation of G0/G1 BrdU-negative cells and G0/G1 BrdU-positive cells (Fig. 6A). This finding suggests that cell division, rather than a repair process occurring in G0/G1 after exposure, was primarily responsible for reducing the frequency of persistent IRIF. These IRIF therefore do not permanently block cell proliferation, which is indeed likely to influence the number of IRIF in the daughter cells. To examine this point in more detail, we analyzed the distribution of G0/G1 BrdU-negative and BrdU-positive cells according to their number of persistent IRIF (Fig. 6B and C). The shape of the distribution in G0/G1 BrdU-negative cells, like the frequency, remained the same between 24 and 48 hours (gray bars in Fig. 6B and C). The proportionately equal decrease for all classes indicates that the number of persistent IRIF per cell did not influence ability to progress through the cell cycle. In addition, the distribution observed for G0/G1 BrdU-positive (compared with G0/G1 BrdU-negative) cells clearly shifted to the classes with fewer IRIF. This result indicates a class change between the mother cell and its daughter cells; daughter cells had fewer persistent IRIF than their mothers. To verify this hypothesis, we blocked cytokinesis with cytochalasin B 48 hours after exposure to 5 Gy. Around half of the binucleated cells had an asymmetric number of persistent IRIF in the daughter nuclei (Fig. 7). Our data thus suggest that the decrease in the frequency of persistent IRIF over time may be linked not to a repair process but rather to a substantially asymmetric distribution of IRIF between daughter cells. Furthermore, this asymmetry suggests that IRIF segregation during anaphase may be abnormal.

To confirm this hypothesis, we analyzed the missegregation events in G0/G1 BrdU positive cells observed at 48 hours after exposure (without cytochalasin B treatment). Among the entire population of G0/G1 BrdU-positive cells, the number of micronuclei and/or nucleoplasmic bridges in mono- and binucleated cells clearly increased and did so dose-dependently (Table 2). More than 85% of these missegregation events were associated with the presence of a γH2AX signal, however; this finding suggests that the structure formed after the passage of a persistent IRI focus across the S and G2 phases may impede the correct segregation of the affected chromosome's sister chromatids (Fig. 8 and Table 2).

4. Discussion

Many studies have described the correlation of transient IRIF with DSBs [5,19,21,22]. ATM phosphorylation of histone H2AX on serine 139 near the break, its amplification over megabases around the break and the resulting observation of nuclear foci have been well described in mammalian cells [6,7,19]. Moreover, this histone modification leads to relaxation of the chromatin architecture, which in turn allows the DNA repair machinery to access the spatially confined region surrounding the break [23–25]. The disappearance of IRIF is generally associated with DSB repair [22] and restoration of the initial chromatin structure [24]. Our data show that, depending on the dose, 5 to 10% of the total IRIF observed at 30 minutes after exposure remain 24 hours after irradiation in 10 to 70% of cells. Relatively few studies have examined the nature and cellular impact of these persistent IRIF. Consistently with the progressive increase of the size of 53BP1 and ATM IRIF reported by Yamauchi *et al* [13], we observed that the area of γH2AX/53BP1 IRIF increased over time as the frequency of γH2AX/53BP1 IRIF decreased (Fig. 1). At 72 hours after exposure, persistent γH2AX IRIF were predominantly large, with areas 2 to 6 times bigger than those measured at 30 minutes (Fig. 2). Some studies suggest that chromatin movement may cause adjacent IRIF to merge, thus contributing to both the reduction of their frequency and their increase in size [26–29]. These observations, however, involved asynchronous cells, in which DSB repair by homologous recombination (HR) can occur when DNA damage is produced during S or G2. In our study, we ensured that DNA damage occurred mainly to cells in G0/G1, thus preventing the use of HR and limiting putative chromatin movements [30]. In this case, persistent γH2AX IRIF may grow larger over time through the amplification of γH2AX signals, probably due to persistent ATM presence at their site [13,15,31,32]. The cause of the persistence and amplification of the phosphorylation nonetheless remains unclear. No repair activity appears to take place at the site of these persistent IRIF [33], although several DNA damage signaling proteins, such as 53BP1 (Fig. 2C), MRE11, and NBS1, co-locate there [32–34]. In addition, and consistent with other studies [32–34], we observed that promyelocytic leukemia nuclear bodies were almost invariably associated with these persistent IRIF (data not shown).

Consistently with the results of Yamauchi *et al* [13], a majority of cells with persistent γH2AX/53BP1 IRIF were halted in G1 until 24 hours after exposure (Fig. 5A). However, analyzing later post-irradiation time points, we observed that this inhibition was not permanent in our model of normal primary endothelial cells (Fig. 4B and 5A). The persistent IRIF analyzed in our study were compatible with cell-cycle progression and were transmitted to daughter cells: HUVECs irradiated in the G0/G1 phase that had persistent IRIF 24 hours after exposure — and not just a few of them — were able to complete a whole cell cycle. Moreover, the ability of cells to progress through a complete cell cycle did not appear to depend on their number of persistent IRIF: between 24 and 48 hours; the frequency of BrdU-negative cells decreased at the same rate, regardless of their number of persistent IRIF (gray bars in Fig. 6B and C).

These observations raise questions about the real nature of these IRIF. Normal cells, such as primary HUVECs, have active cell-cycle checkpoints able to block the cycle's progression until the resolution of DSBs [35–37]. Thus, if persistent IRIF correspond to a somehow stabilized unrejoined DSB, our

observations would seem to indicate that this mechanism failed to detect this structure. Several studies suggest that the G1/S phase checkpoint can be bypassed, despite unrepaired DSBs, particularly if cells are in the late G1 phase during irradiation and have passed a point where they can no longer initiate a global shutdown of the S phase [38]. This hypothesis seems unlikely in our case, as it would mean that this restriction point would have been passed 24 hours before the cells entered the S phase. Moreover, DSBs induced in the G0/G1 phase can also persist after DNA replication, as shown by G2 premature chromosome condensation assays combined with FISH using pantelomeric PNA probes [39]. In this case, the observation of incomplete chromosome elements (chromosome fragments without a telomere signal at each end) demonstrated the presence at G2 phase of unrejoined chromosome breaks from DSBs induced in the G0/G1 phase. Another study reported the presence in G2 phase of chromosome breaks (without discriminating complete from incomplete chromosome elements) and γH2AX IRIF in fibroblasts irradiated in the G0/G1 phase [40]. On the other hand, the G2/M checkpoint appears to induce a drastic reduction in the rate of incomplete chromosome elements in M-phase cells [39], although the rate of incomplete chromosome elements per cell in M phase remains dose-dependent. The selection that appears to occur during the G2/M transition may be consistent with the difference in the frequency of persistent IRIF observed in our experiments between G0/G1 BrdU-negative cells and G0/G1 BrdU-positive cells (Fig. 6A). However, the absence of any significant arrest in G2 in our model suggests that this mechanism may not apply here (Fig. 4A).

Thus if these incomplete chromosome elements are able to reach cytokinesis, they should be transmitted to daughter cells, as were the persistent IRIF observed in our study. Analyzing metaphase cells, Martin *et al.* reported that persistent IRIF do not seem to co-locate with either telomere-free chromosome ends or misrepaired breaks [41]. It is nonetheless important to note that histone H2AX phosphorylation takes place on serine 139 along the chromosome arms from metaphase to telophase, independently of any DNA damage induced [42–44]. Thus, it appears difficult, or even impossible, to distinguish clearly between the H2AX phosphorylation that occurs normally during M phase and that induced by DDR.

Nevertheless, the asymmetric distribution of persistent IRIF between daughter cells (Fig. 7) suggests that it may be difficult for this structure to segregate correctly during anaphase. The normal distribution of chromosomes between daughter cells is driven by the presence of a centromere that allows sister chromatids to segregate equally in each cell [45,46]. Thus, the structure formed after the passage of a persistent IRI focus across the S and G2 phases may impede the correct segregation of the affected chromosome's sister chromatids. The rate of missegregation associated with the presence of a γH2AX signal strongly supports this hypothesis (Table 2 and Fig. 8). All these observations suggest that the nature of the IRIF must differ at least slightly before and after the first cell division following exposure. If DNA damage is induced in G0/G1 phase but the cell nonetheless reaches metaphase, the process of chromosome segregation during anaphase may encounter numerous problems, including the conversion of a remaining DSB into chromosome breaks (CRB) (Fig. 9). This transition into CRBs of DSBs induced in the G1 phase and reaching metaphase has been described in yeast where two types of associations may

occur: one between the two sides of the DNA break (intrachromosomal association) and the other between sister chromosomal fragments from either side of the DNA break (interchromosomal association) [47]. These two associations lead to a kind of “tug-of-war” between the two spindle poles during the anaphase, which almost always results in co-segregation of the acentric chromosome fragments [47]. According to this model, the persistent IRIF observed after cellular division in our study might correspond to several kinds of atypical chromosomal structures composed of segregated chromatids with unrejoined DSBs either stabilized or converted into CRBs. These chromosome elements may be included in the cell nucleus or may form micronuclei (Fig. 9).

In conclusion, we observed that cells containing persistent IRIF do not block the cell cycle permanently and that these IRIF can be transmitted to daughter cells. Moreover the asymmetric distribution of persistent IRIF between daughter cells indicates that cell division likely affects the structure signaled by persistent IRIF and may lead to the formation of an atypical chromosomal structure in daughter cells. This atypical chromosomal assembly may be lethal or result in gene dosage imbalance and possibly enhanced genomic instability in daughter cells. The consequences of this phenomenon should be further analyzed, especially as more than 50% of the progeny of cells exposed to 5 Gy of irradiation (10% for 1 Gy) may carry this abnormal structure.

Conflict of interest

None

Acknowledgments

The authors would like to thank C. Baldeyron and M. Benderitter for their constructive comments. The authors would also like to thank M. Baumann, Y. Ristic, and L. Van Ryckeghem for performing the radiation exposure with the Elekta Synergy Platform and the related dosimetry. The authors gratefully acknowledge the financial assistance awarded by “Electricité de France” (EDF).

References

[1] M. Löbrich, P.A. Jeggo, The impact of a negligent G2/M checkpoint on genomic instability and cancer induction., Nat. Rev. Cancer. 7 (2007) 861–9. doi:10.1038/nrc2248.

[2] S. Burma, B.P. Chen, M. Murphy, A. Kurimasa, D.J. Chen, ATM phosphorylates histone H2AX in response to DNA double-strand breaks., J. Biol. Chem. 276 (2001) 42462–42467. doi:10.1074/jbc.C100466200.

[3] T. Stiff, M. O'Driscoll, N. Rief, K. Iwabuchi, M. Löbrich, P.A. Jeggo, ATM and DNA-PK Function Redundantly to Phosphorylate H2AX after Exposure to Ionizing Radiation, Cancer Res. 64 (2004) 2390–2396. doi:10.1158/0008-5472.CAN-03-3207.

[4] C.J. Bakkenist, M.B. Kastan, DNA damage activates ATM through intermolecular autophosphorylation and dimer dissociation., Nature. 421 (2003) 499–506. doi:10.1038/nature01368.

[5] E.P. Rogakou, D.R. Pilch, A.H. Orr, V.S. Ivanova, W.M. Bonner, DNA double-stranded breaks induce histone H2AX phosphorylation on serine 139., J. Biol. Chem. 273 (1998) 5858–68. doi:10.1074/jbc.273.10.5858.

[6] E.P. Rogakou, C. Boon, C. Redon, W.M. Bonner, Megabase chromatin domains involved in DNA double-strand breaks in vivo., J. Cell Biol. 146 (1999) 905–16. doi:10.1083/jcb.146.5.905.

[7] A. Kinner, W. Wu, C. Staudt, G. Iliakis, Gamma-H2AX in recognition and signaling of DNA double-strand breaks in the context of chromatin., Nucleic Acids Res. 36 (2008) 5678–5694. doi:10.1093/nar/gkn550.

[8] H. van Attikum, S.M. Gasser, Crosstalk between histone modifications during the DNA damage response., Trends Cell Biol. 19 (2009) 207–17. doi:10.1016/j.tcb.2009.03.001.

[9] M. Lisby, R. Rothstein, Choreography of recombination proteins during the DNA damage response, DNA Repair (Amst). 8 (2009) 1068–1076. doi:10.1016/j.dnarep.2009.04.007.

[10] T.T. Paull, E.P. Rogakou, V. Yamazaki, C.U. Kirchgessner, M. Gellert, W.M. Bonner, A critical role for histone H2AX in recruitment of repair factors to nuclear foci after DNA damage, Curr. Biol. 10 (2000) 886–895. doi:10.1016/S0960-9822(00)00610-2.

[11] M.C. Keogh, J.A. Kim, M. Downey, J. Fillingham, D. Chowdhury, J.C. Harrison, et al., A phosphatase complex that dephosphorylates gammaH2AX regulates DNA damage checkpoint recovery., Nature. 439 (2006) 497–501. doi:10.1038/nature04772.

[12] D. Chowdhury, M.C. Keogh, H. Ishii, C.L. Peterson, S. Buratowski, J. Lieberman, gamma-H2AX dephosphorylation by protein phosphatase 2A facilitates DNA double-strand break repair., Mol. Cell. 20 (2005) 801–809. doi:10.1016/j.molcel.2005.10.003.

[13] M. Yamauchi, Y. Oka, M. Yamamoto, K. Niimura, M. Uchida, S. Kodama, et al., Growth of persistent foci of DNA damage checkpoint factors is essential for amplification of G1 checkpoint signaling, DNA Repair (Amst). 7 (2008) 405–417. doi:10.1016/j.dnarep.2007.11.011.

[14] F. d'Adda di Fagagna, P.M. Reaper, L. Clay-Farrace, H. Fiegler, P. Carr, T. Von Zglinicki, et al., A DNA damage checkpoint response in telomere-initiated senescence., Nature. 426 (2003) 194–8. doi:10.1038/nature02118.

[15] F. Rodier, J.P. Coppé, C.K. Patil, W.A.M. Hoeijmakers, D.P. Muñoz, S.R. Raza, et al., Persistent DNA damage signalling triggers senescence-associated inflammatory cytokine secretion., Nat. Cell

Biol. 11 (2009) 973–9. doi:10.1038/ncb1909.

[16] S. Yang, C. Kuo, J.E. Bisi, M.K. Kim, PML-dependent apoptosis after DNA damage is regulated by the checkpoint kinase hCds1/Chk2., Nat. Cell Biol. 4 (2002) 865–870. doi:10.1038/ncb869.

[17] G. Gruel, C. Villagrasa, P. Voisin, I. Clairand, M. Benderitter, J.-F. Bottollier-Depois, et al., Cell to Cell Variability of Radiation-Induced Foci: Relation between Observed Damage and Energy Deposition., PLoS One. 11 (2016) e0145786. doi:10.1371/journal.pone.0145786.

[18] J. Canny, A computational approach to edge detection., IEEE Trans. Pattern Anal. Mach. Intell. 8 (1986) 679–98. doi:10.1007/s11263-010-0392-0.

[19] M. Löbrich, A. Shibata, A. Beucher, A. Fisher, M. Ensminger, A.A. Goodarzi, et al., γH2AX foci analysis for monitoring DNA double-strand break repair: Strengths, limitations and optimization, Cell Cycle. 9 (2010) 662–669. doi:10.4161/cc.9.4.10764.

[20] S. V Costes, I. Chiolo, J.M. Pluth, M.H. Barcellos-Hoff, B. Jakob, Spatiotemporal characterization of ionizing radiation induced DNA damage foci and their relation to chromatin organization., Mutat. Res. 704 (2010) 78–87. doi:10.1016/j.mrrev.2009.12.006.

[21] O.A. Sedelnikova, I. Horikawa, D.B. Zimonjic, N.C. Popescu, W.M. Bonner, J.C. Barrett, Senescing human cells and ageing mice accumulate DNA lesions with unrepairable double-strand breaks., Nat. Cell Biol. 6 (2004) 168–70. doi:10.1038/ncb1095.

[22] K. Rothkamm, M. Löbrich, Evidence for a lack of DNA double-strand break repair in human cells exposed to very low x-ray doses., Proc. Natl. Acad. Sci. U. S. A. 100 (2003) 5057–62. doi:10.1073/pnas.0830918100.

[23] T. Misteli, E. Soutoglou, The emerging role of nuclear architecture in DNA repair and genome maintenance., Nat. Rev. Mol. Cell Biol. 10 (2009) 243–254. doi:10.1038/nrm2651.

[24] G. Soria, S.E. Polo, G. Almouzni, Prime, Repair, Restore: The Active Role of Chromatin in the DNA Damage Response, Mol. Cell. 46 (2012) 722–734. doi:10.1016/j.molcel.2012.06.002.

[25] B.D. Price, A.D. D'Andrea, Chromatin remodeling at DNA double-strand breaks, Cell. 152 (2013) 1344–1354. doi:10.1016/j.cell.2013.02.011.

[26] B. Jakob, J. Splinter, M. Durante, G. Taucher-Scholz, Live cell microscopy analysis of radiation-induced DNA double-strand break motion., Proc. Natl. Acad. Sci. U. S. A. 106 (2009) 3172–7. doi:10.1073/pnas.0810987106.

[27] W. Georgescu, A. Osseiran, M. Rojec, Y. Liu, M. Bombrun, J. Tang, et al., Characterizing the DNA Damage Response by Cell Tracking Algorithms and Cell Features Classification Using High-Content Time-Lapse Analysis., PLoS One. 10 (2015) e0129438. doi:10.1371/journal.pone.0129438.

[28] I. Chiolo, A. Minoda, S.U. Colmenares, A. Polyzos, S. V Costes, G.H. Karpen, Double-strand breaks in heterochromatin move outside of a dynamic HP1a domain to complete recombinational

repair., Cell. 144 (2011) 732–44. doi:10.1016/j.cell.2011.02.012.

[29] M.J. Kruhlak, A. Celeste, G. Dellaire, O. Fernandez-Capetillo, W.G. Müller, J.G. McNally, et al., Changes in chromatin structure and mobility in living cells at sites of DNA double-strand breaks., J. Cell Biol. 172 (2006) 823–34. doi:10.1083/jcb.200510015.

[30] E. Soutoglou, J.F. Dorn, K. Sengupta, M. Jasin, A. Nussenzweig, T. Ried, et al., Positional stability of single double-strand breaks in mammalian cells., Nat. Cell Biol. 9 (2007) 675–82. doi:10.1038/ncb1591.

[31] M. Suzuki, K. Suzuki, S. Kodama, M. Watanabe, Phosphorylated histone H2AX foci persist on rejoined mitotic chromosomes in normal human diploid cells exposed to ionizing radiation., Radiat. Res. 165 (2006) 269–276. doi:10.1667/RR3508.1.

[32] G. Dellaire, R.W. Ching, K. Ahmed, F. Jalali, K.C.K. Tse, R.G. Bristow, et al., Promyelocytic leukemia nuclear bodies behave as DNA damage sensors whose response to DNA double-strand breaks is regulated by NBS1 and the kinases ATM, Chk2, and ATR, J. Cell Biol. 175 (2006) 55–66. doi:10.1083/jcb.200604009.

[33] F. Rodier, D.P. Muñoz, R. Teachenor, V. Chu, O. Le, D. Bhaumik, et al., DNA-SCARS: distinct nuclear structures that sustain damage-induced senescence growth arrest and inflammatory cytokine secretion., J. Cell Sci. 124 (2011) 68–81. doi:10.1242/jcs.071340.

[34] R. Carbone, M. Pearson, S. Minucci, P.G. Pelicci, PML NBs associate with the hMre11 complex and p53 at sites of irradiation induced DNA damage., Oncogene. 21 (2002) 1633–1640. doi:10.1038/sj.onc.1205227.

[35] G.K. Dasika, S.C. Lin, S. Zhao, P. Sung, A. Tomkinson, E.Y. Lee, DNA damage-induced cell cycle checkpoints and DNA strand break repair in development and tumorigenesis., Oncogene. 18 (1999) 7883–99. doi:10.1038/sj.onc.1203283.

[36] B.B. Zhou, S.J. Elledge, The DNA damage response: putting checkpoints in perspective., Nature. 408 (2000) 433–9. doi:10.1038/35044005.

[37] D.C. van Gent, J.H. Hoeijmakers, R. Kanaar, Chromosomal stability and the DNA double-stranded break connection., Nat. Rev. Genet. 2 (2001) 196–206. doi:10.1038/35056049.

[38] K.L. Cann, G.G. Hicks, Absence of an immediate G1/S checkpoint in primary MEFs following gamma-irradiation identifies a novel checkpoint switch., Cell Cycle. 5 (2006) 1823–30. doi:10.4161/cc.5.16.3009.

[39] P. Rodríguez, J.F. Barquinero, A. Duran, M.R. Caballín, M. Ribas, L. Barrios, Cells bearing chromosome aberrations lacking one telomere are selectively blocked at the G2/M checkpoint, Mutat. Res. - Fundam. Mol. Mech. Mutagen. 670 (2009) 53–58. doi:10.1016/j.mrfmmm.2009.07.003.

[40] D. Deckbar, T. Stiff, B. Koch, C. Reis, M. Löbrich, P.A. Jeggo, The limitations of the G1-S

checkpoint, Cancer Res. 70 (2010) 4412–4421. doi:10.1158/0008-5472.CAN-09-3198.

[41] M. Martín, M. Terradas, L. Hernández, A. Genescà, γH2AX foci on apparently intact mitotic chromosomes: Not signatures of misrejoining events but signals of unresolved DNA damage., Cell Cycle. 13 (2014) 3026–36. doi:10.4161/15384101.2014.947786.

[42] K.J. McManus, M.J. Hendzel, ATM-dependent DNA damage-independent mitotic phosphorylation of H2AX in normally growing mammalian cells., Mol. Biol. Cell. 16 (2005) 5013–25. doi:10.1091/mbc.E05-01-0065.

[43] Y. Ichijima, R. Sakasai, N. Okita, K. Asahina, S. Mizutani, H. Teraoka, Phosphorylation of histone H2AX at M phase in human cells without DNA damage response., Biochem. Biophys. Res. Commun. 336 (2005) 807–12. doi:10.1016/j.bbrc.2005.08.164.

[44] V. Turinetto, C. Giachino, Multiple facets of histone variant H2AX: a DNA double-strand-break marker with several biological functions., Nucleic Acids Res. 43 (2015) 2489–98. doi:10.1093/nar/gkv061.

[45] J. Zhou, J. Yao, H.C. Joshi, Attachment and tension in the spindle assembly checkpoint., J. Cell Sci. 115 (2002) 3547–3555. doi:10.1242/jcs.00029.

[46] A. Musacchio, E.D. Salmon, The spindle-assembly checkpoint in space and time., Nat. Rev. Mol. Cell Biol. 8 (2007) 379–93. doi:10.1038/nrm2163.

[47] J.A. Kaye, J.A. Melo, S.K. Cheung, M.B. Vaze, J.E. Haber, D.P. Toczyski, DNA breaks promote genomic instability by impeding proper chromosome segregation., Curr. Biol. 14 (2004) 2096–106. doi:10.1016/j.cub.2004.10.051.

Figure Legends

Fig. 1. Numbers and areas of γH2AX foci in G0/G1 primary HUVECs as a function of time after irradiation by 1 Gy (light gray boxes), 5 Gy (dark gray boxes), and in non-irradiated cells (white boxes). Box-and-whisker plots of (A) the number of γH2AX foci per nucleus, and (B) their corresponding areas. Bold black bars of boxplots correspond to medians. The lower and upper borders of the box correspond to the first and third quartiles, respectively, and the upper and lower whiskers to 1.5 times the interquartile distance. The numbers of γH2AX foci per nuclei and their respective areas were evaluated with image analysis software on around 3,000 cells for each post-irradiation time, corresponding to one representative experiment. The number of γH2AX IRIF peaked 30 minutes post-exposure. The area of γH2AX IRIF increased as the number per nucleus decreased. Most early γH2AX IRIF (before 24 hours after exposure) were small, but persistent IRIF were characterized by a larger size.

Fig. 2. Distribution of IRIF area in G0/G1 cells after X-ray exposure at 1 Gy. Frequencies of γH2AX foci area at (A) 30 minutes and (B) 72 hours after irradiation were normalized relative to the corresponding non-irradiated condition to define the different ranges of size observed for early and persistent IRIF. Because spontaneous foci are also present in irradiated cells, to focus only on the size of IRIF (foci induced by irradiation), we normalized them, that is, calculated a ratio (irradiated versus control) of the frequency of each class of the size distribution. The results shown are obtained by pooling the data of 5 experiments and correspond to the analysis of the distribution of size of about 460,000 IRIF at 30 minutes and 21,000 IRIF at 72 hours after irradiation. Early IRIF were characterized by an area ranging from 0.2 to 1.3 μm^2 and persistent IRIF by an area greater than 1.1 μm^2. (C) Representative pictures of the co-labeling by immunofluorescence of γH2AX (FITC) and 53BP1 (Alexa Fluor® 594) corresponding to early (upper panel, 30 min) and persistent (lower panel, 72 h) IRIF in HUVECs. DNA was stained with DAPI. We observed co-location of γH2AX and 53BP1 IRIF for both early and persistent IRIF. Scale bar corresponds to 10 µm.

Fig. 3. The proportion of G0/G1 cells with at least one persistent IRI focus as a function of time since exposure. The analyses were performed on cells exposed to irradiation of 1 Gy (light gray triangles) and 5 Gy (dark gray squares) and on unirradiated cells (white diamonds). The mean percentages of cells with at least one persistent γH2AX focus ± standard error (s.e.) were calculated from at least 5 experiments. For each condition, the average number of analyzed cells ranged from about 1,300 to 11,000. The decrease in the percentage of cells with persistent IRIF was more pronounced for those irradiated by 5 Gy, compared with 1 Gy, about 6% per 24 hours for 5 Gy and only 1% per 24 hours for 1 Gy.

Fig.4. Persistent IRIF and cell proliferation. (A-B) To study the evolution of cell division after irradiation, we added BrdU just after exposure. Cells in the different phases of the cell cycle were selected by assessment of the integrated intensity of the DAPI signal (DNA content) combined with the integrated intensity of γH2AX signal in the entire nucleus (S phase). Percentages of cells in each phase of the cell cycle were measured at 24 hours (A) and 48 hours after irradiation (B) on unirradiated cells (white bars) and on cells exposed to 1 Gy (light gray bars) and 5 Gy (dark gray bars). The mean percentages ± s.e. were calculated from the results of 5 experiments, with an average of about 3,000 cells analyzed per condition. (C) The density of the cell monolayer was evaluated at different time points after exposure for unirradiated cells (white diamonds) and for cells exposed to 1 Gy (light gray triangles) and 5 Gy (dark gray squares). The cell monolayer density was measured by counting of the number of nuclei per cm^2 observed at different time points after exposure. These measurements were performed on around 5,000 images per condition. The percentages were calculated for each condition with respect to the density measured 10 min after exposure. The percentages and error bars correspond to the calculation of means and standard errors based on 4 experiments.

Fig. 5. Persistent IRIF do not permanently block cell proliferation. To recognize cells that had completed a full cell cycle since irradiation, we added BrdU just after exposure and considered only G0/G1 cells. (A) Histograms of the proportion of G0/G1 cells as a function of BrdU incorporation (BrdU+ in light gray and BrdU- in white) and presence (dotted) or not (empty) of persistent IRIF. The percentages were calculated for unirradiated cells, respectively 5, 24 and 48 hours after the addition of BrdU, and for irradiated cells, respectively, 24 and 48 hours after exposure to 1 and 5 Gy and the addition of BrdU. The mean percentages were calculated from the results of 3 experiments, with an average of about 3,000 cells analyzed per condition. (B) Representative pictures of the co-labeling by immunofluorescence of γH2AX, BrdU, and 53BP1 performed 48 hours after 5-Gy irradiation, using primary antibodies against γH2AX, BrdU, and 53BP1, detected respectively by secondary antibodies conjugated to FITC, Alexa Fluor® 594, and Alexa Fluor® 647. DNA was stained with DAPI. Persistent γH2AX/53BP1 IRIF were observed in G0/G1 BrdU-positive cells. Scale bar corresponds to 10 µm.

Fig. 6. Average numbers and distribution of persistent IRIF per cell in G0/G1 BrdU-positive and BrdU-negative cells. We evaluated the number of persistent γH2AX IRIF in G0/G1 BrdU-positive versus G0/G1 BrdU-negative cells in the G0/G1 phase. (A) Average number of persistent IRIF per cell analyzed 24 hours (dark gray bars) and 48 hours (light gray bars) after exposure to 5 Gy of X-rays. The frequency of persistent IRIF remained stable over time in each subpopulation of G0/G1 BrdU-negative cells and G0/G1 BrdU-positive cells. The reduced frequency of persistent IRIF appears to be associated mainly with cell division rather than time since exposure. The mean number ± s.e. was calculated from the results of 3 experiments; for each condition the average number of analyzed cells ranged from about 3,000 to 14,000. Student's test: ** $\alpha < 0.025$ and *** $\alpha < 0.01$. (B-C) Percentages of cells with each number of persistent IRIF were calculated in G0/G1 BrdU-positive (black bars) and G0/G1 BrdU-negative (gray bars) cells at (B) 24 hours and (C) 48 hours after exposure to 5 Gy irradiation. The shape of the distribution observed in G0/G1 BrdU-negative cells (gray bars) remained the same at (B) 24 hours and (C) 48 hours. The proportionately equal decrease for all classes indicated that all had the same ability to go through the cell cycle regardless of the number of persistent IRIF per cell. The distribution observed for G0/G1 BrdU-positive cells shifted to lower classes (i.e., cells with fewer IRIF) compared to G0/G1 BrdU-negative cells. This result indicates a class change between the mother and daughter cells; the daughter cells have fewer persistent IRIF than the mother. Percentages were calculated after pooling the data from 3 independent experiments corresponding to analysis of 3,000 to 14,000 cells, depending on the cell subpopulation ($BrdU^+$ or $BrdU^-$) and time since exposure.

Fig. 7. Distribution of persistent IRIF between daughter cells. At 48 hours after exposure to 5 Gy, we blocked cytokinesis by adding cytochalasin B to cell culture medium; 24 hours later, we immunostained the cells with an antibody against γH2AX and stained the DNA with DAPI. Representative pictures of the immunofluorescence labeling of γH2AX of binucleated cells with a difference of 0 (left panel), 1 (middle

panel), and 2 (right panel) persistent IRIF between the two daughter nuclei. Scale bar corresponds to 10 µm. The percentage of binucleated cell with a difference of 0, 1, or 2 persistent IRIF between the two daughter nuclei was estimated from 3 independent experiments (around 100 binucleated cells for each). Around half of the binucleated cells had an asymmetric number of persistent IRIF in the daughter nuclei.

Fig. 8. Persistent IRIF induce missegregation phenotypes in BrdU-positive cells. Representative pictures of BrdU-positive cells with different kinds of missegregation observed 48 hours after irradiation, with primary antibodies against γH2AX and BrdU (not shown), detected respectively by secondary antibodies conjugated to FITC and Alexa Fluor® 594. DNA was stained with DAPI. (A) binucleated cells including a micronucleus and a nucleoplasmic bridge or a broken nucleoplasmic bridge with a γH2AX signal. (B) G0/G1 cells including a micronucleus with a γH2AX signal. (C) G0/G1 cells including a broken nucleoplasmic bridge with a γH2AX signal. Scale bar corresponds to 10 µm.

Fig. 9. Model of inheritance of one persistent IRIF based on the hypothesis of an unrepaired DSB. The two broken ends of a DSB are maintained close by non-homologous end-joining repair proteins (intrachromosomal association; purple circles). After DNA replication, association between sister chromosomal fragments from either side of the DNA break can occur (interchromosomal association; orange circles) [47]. The structure formed after the passage of a persistent IRI focus across the S and G2 phases may impede the correct segregation of affected chromosome's sister chromatids. Consequently, the nature of IRIF in the nucleus of daughter cells might differ before and after the first cell division. Thus, the IRIF observed in daughter cells might correspond to several atypical chromosomal structures resulting from abnormal anaphase resolution.

Fig. 1

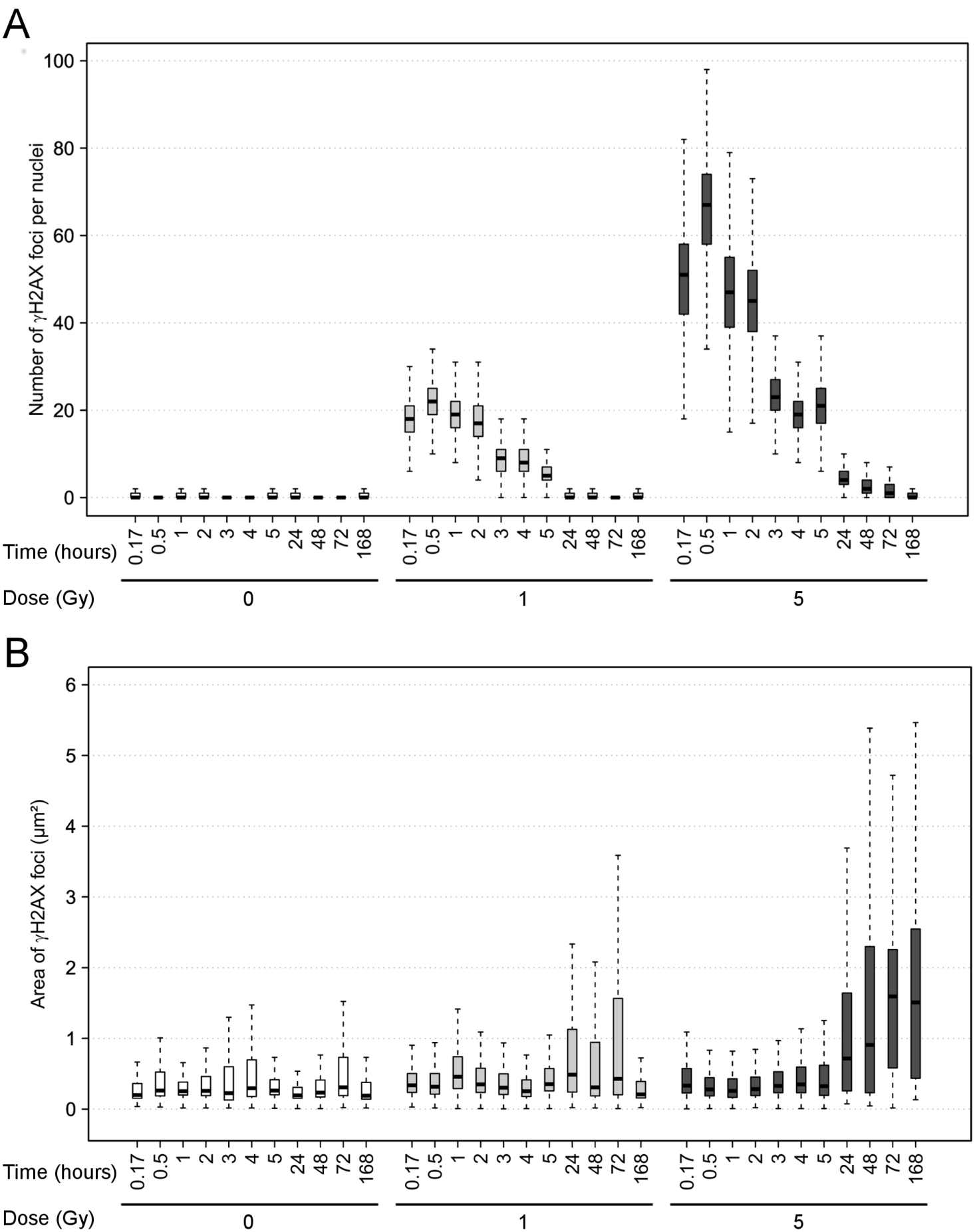
A
Number of γH2AX foci per nuclei
0
20
40
60
80
100
Time (hours)
0.17
0.5
1
2
3
4
5
24
48
72
168
Dose (Gy)
0
1
5
B
Area of γH2AX foci (μm²)
0
1
2
3
4
5
6
Time (hours)
0.17
0.5
1
2
3
4
5
24
48
72
168
Dose (Gy)
0
1
5

Fig. 2

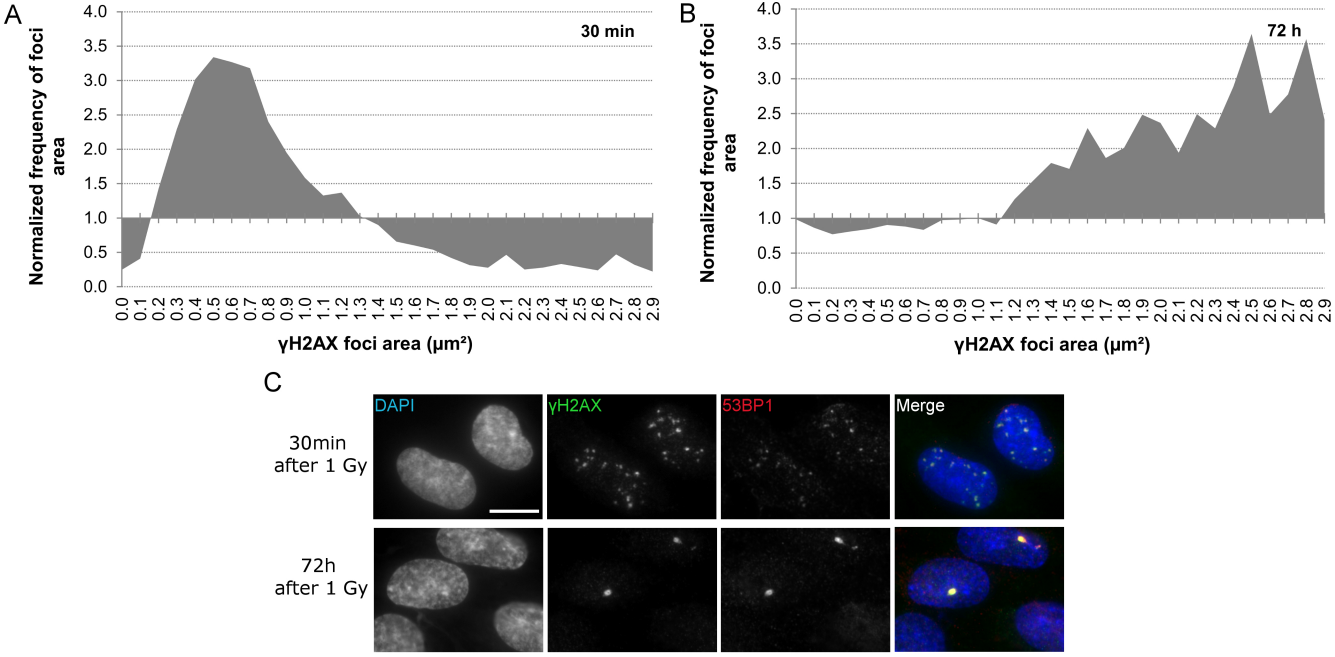
A
30 min
Normalized frequency of foci area
γH2AX foci area (μm²)
B
72 h
Normalized frequency of foci area
γH2AX foci area (μm²)
C
DAPI
γH2AX
53BP1
Merge
30min after 1 Gy
72h after 1 Gy

Fig. 3

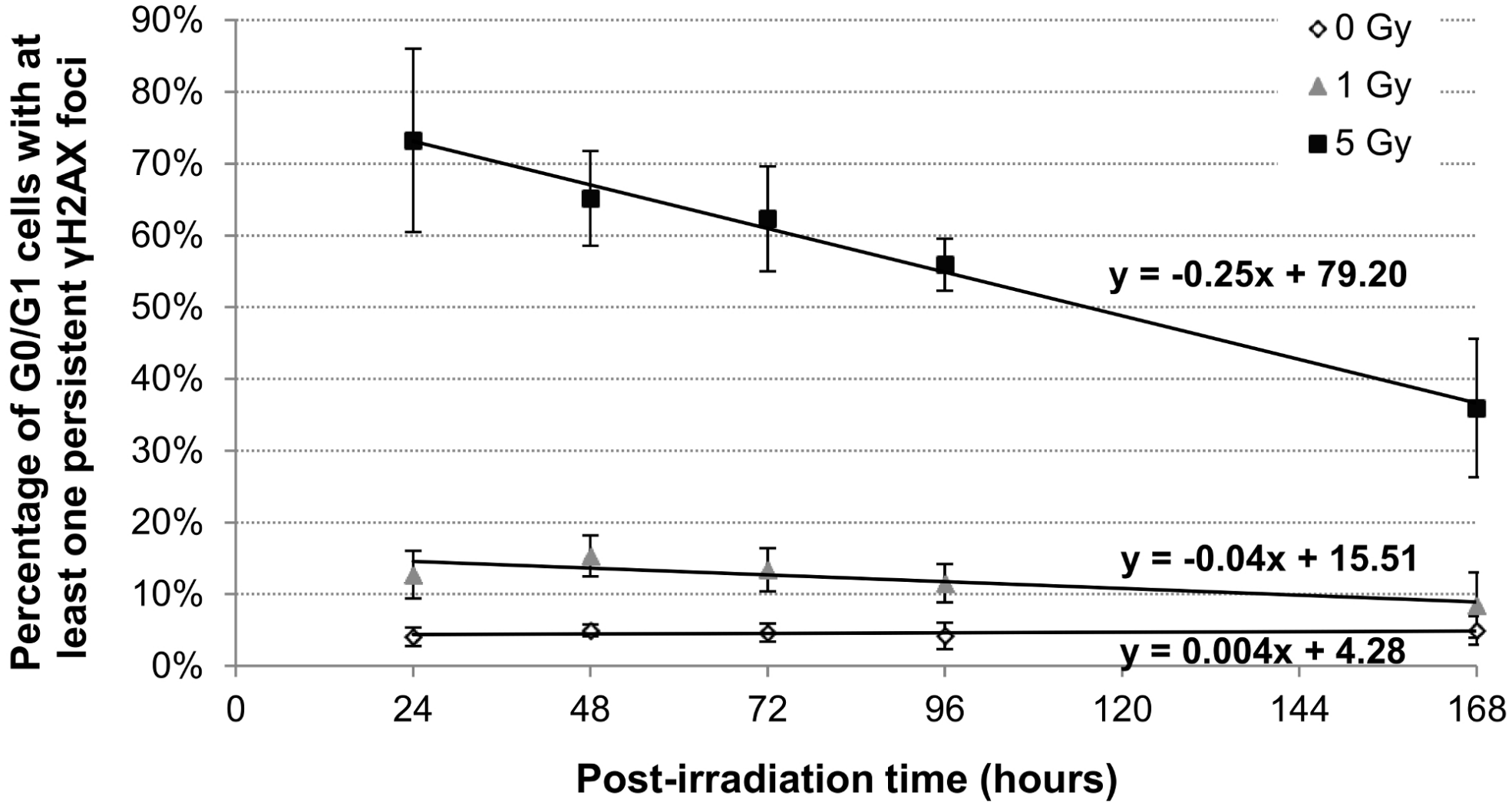
Percentage of G0/G1 cells with at least one persistent γH2AX foci
90%
80%
70%
60%
50%
40%
30%
20%
10%
0%
0 Gy
1 Gy
5 Gy
y = -0.25x + 79.20
y = -0.04x + 15.51
y = 0.004x + 4.28
0
24
48
72
96
120
144
168
Post-irradiation time (hours)

Fig. 4

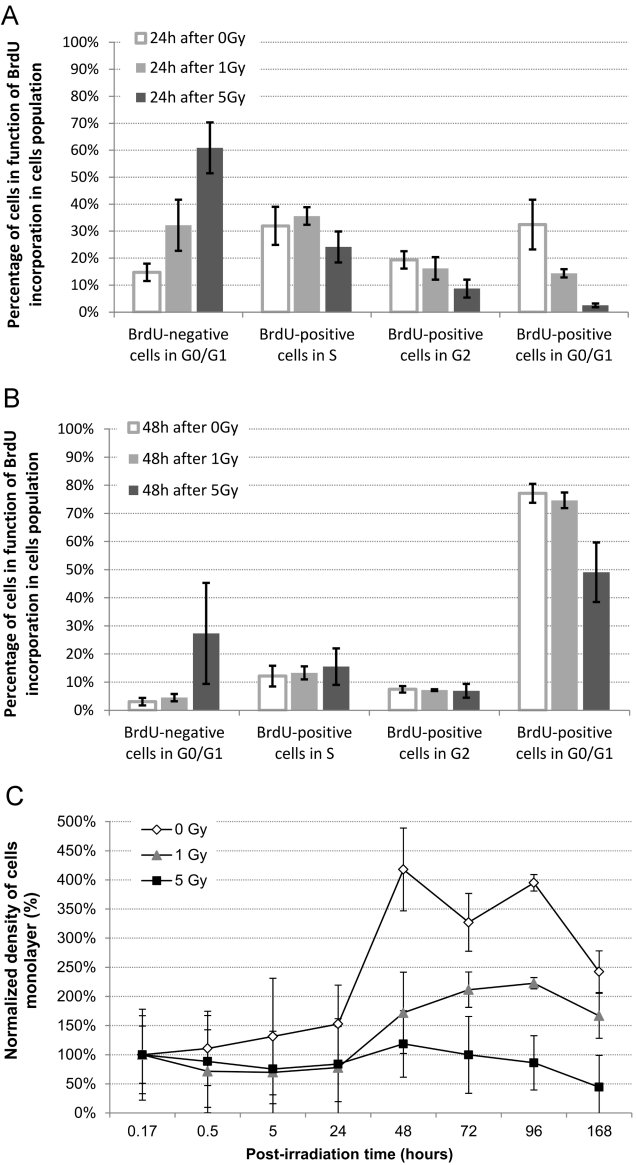
A
24h after 0Gy
24h after 1Gy
24h after 5Gy
Percentage of cells in function of BrdU incorporation in cells population
100%
90%
80%
70%
60%
50%
40%
30%
20%
10%
0%
BrdU-negative cells in G0/G1
BrdU-positive cells in S
BrdU-positive cells in G2
BrdU-positive cells in G0/G1
B
48h after 0Gy
48h after 1Gy
48h after 5Gy
Percentage of cells in function of BrdU incorporation in cells population
BrdU-negative cells in G0/G1
BrdU-positive cells in S
BrdU-positive cells in G2
BrdU-positive cells in G0/G1
C
0 Gy
1 Gy
5 Gy
Normalized density of cells monolayer (%)
500%
450%
400%
350%
300%
250%
200%
150%
100%
50%
0%
0.17
0.5
5
24
48
72
96
168
Post-irradiation time (hours)

Fig. 5

A

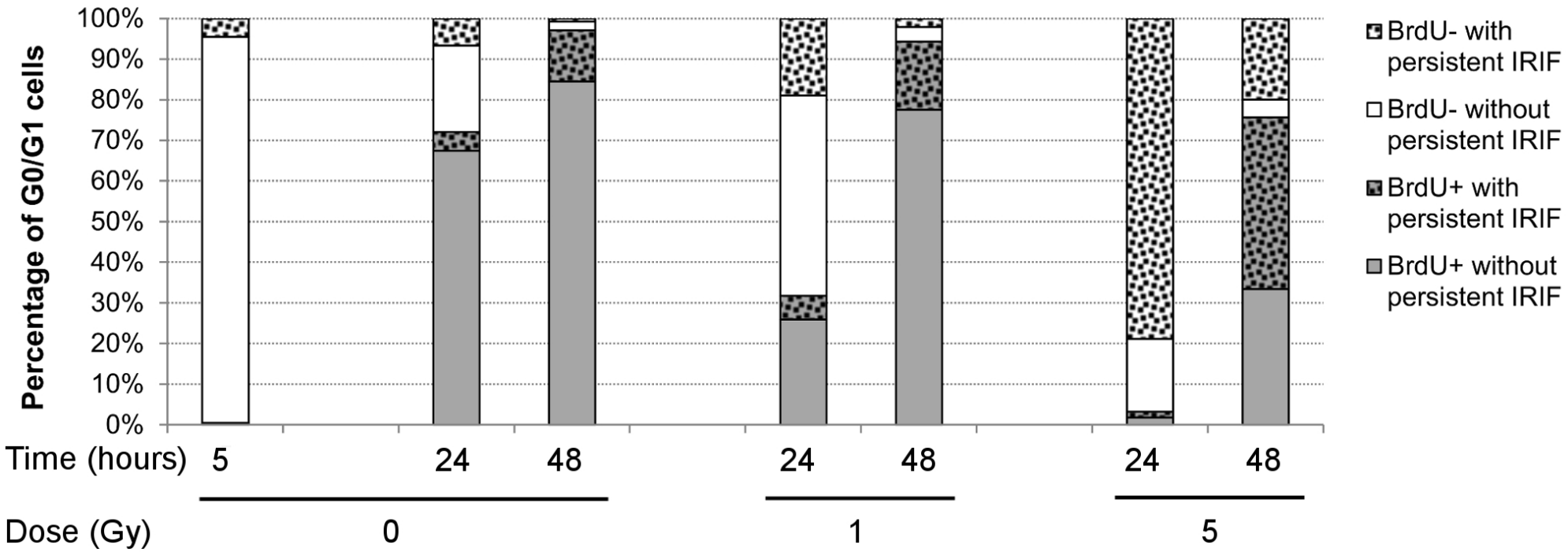
Percentage of G0/G1 cells
100%
90%
80%
70%
60%
50%
40%
30%
20%
10%
0%
Time (hours)
5
24
48
24
48
24
48
Dose (Gy)
0
1
5
BrdU- with persistent IRIF
BrdU- without persistent IRIF
BrdU+ with persistent IRIF
BrdU+ without persistent IRIF

B

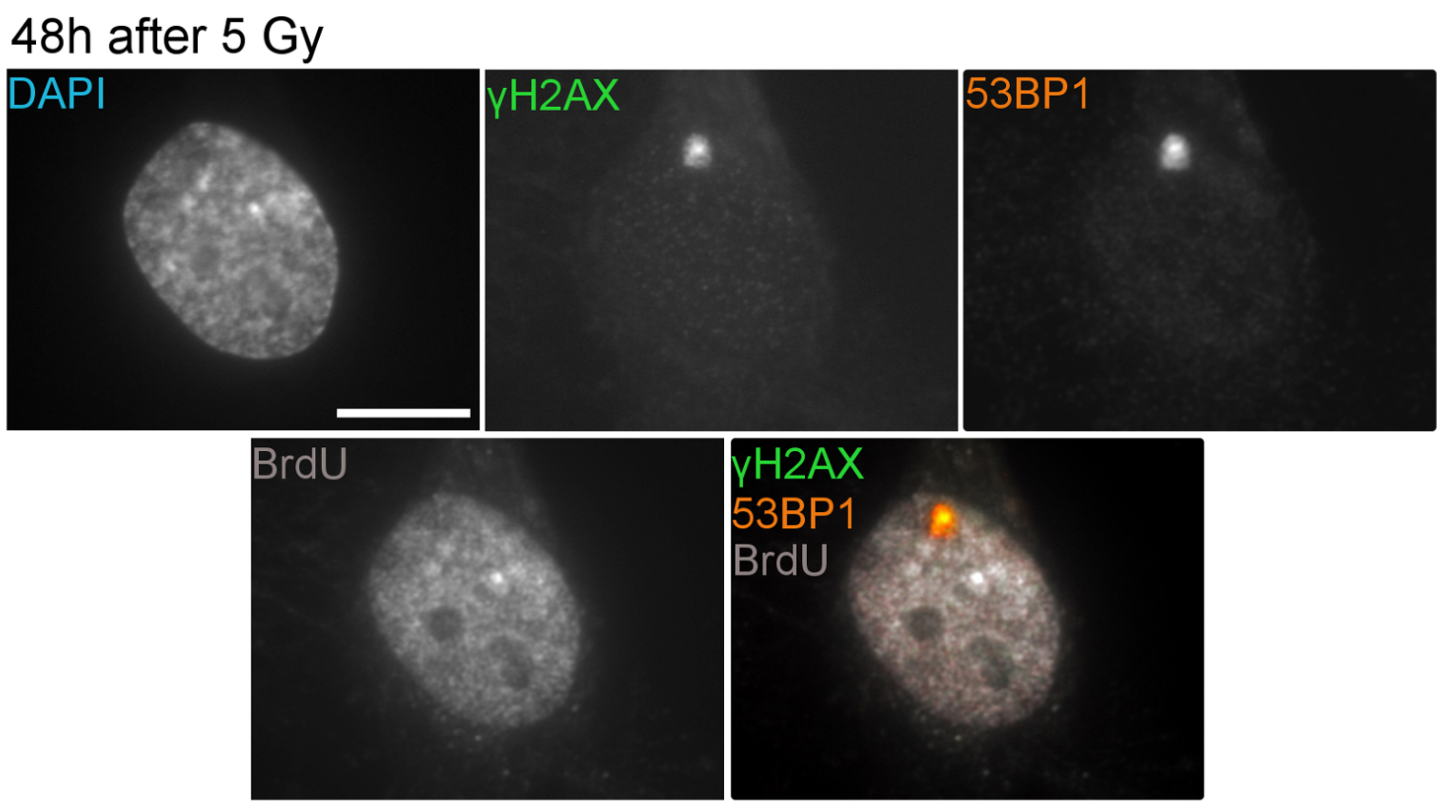
48h after 5 Gy
DAPI
γH2AX
53BP1
BrdU
γH2AX
53BP1
BrdU

Fig. 6

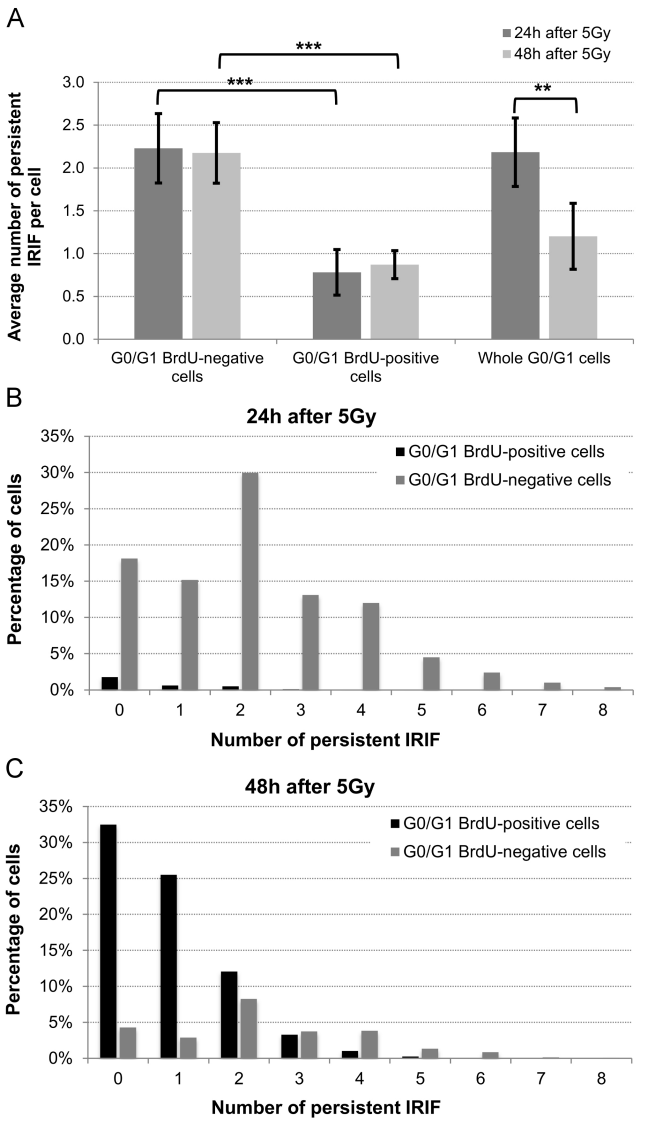
A
24h after 5Gy
48h after 5Gy
***
***
**
Average number of persistent IRIF per cell
3.0
2.5
2.0
1.5
1.0
0.5
0.0
G0/G1 BrdU-negative cells
G0/G1 BrdU-positive cells
Whole G0/G1 cells
B
24h after 5Gy
G0/G1 BrdU-positive cells
G0/G1 BrdU-negative cells
Percentage of cells
35%
30%
25%
20%
15%
10%
5%
0%
0
1
2
3
4
5
6
7
8
Number of persistent IRIF
C
48h after 5Gy
G0/G1 BrdU-positive cells
G0/G1 BrdU-negative cells
Percentage of cells
35%
30%
25%
20%
15%
10%
5%
0%
0
1
2
3
4
5
6
7
8
Number of persistent IRIF

Fig. 7

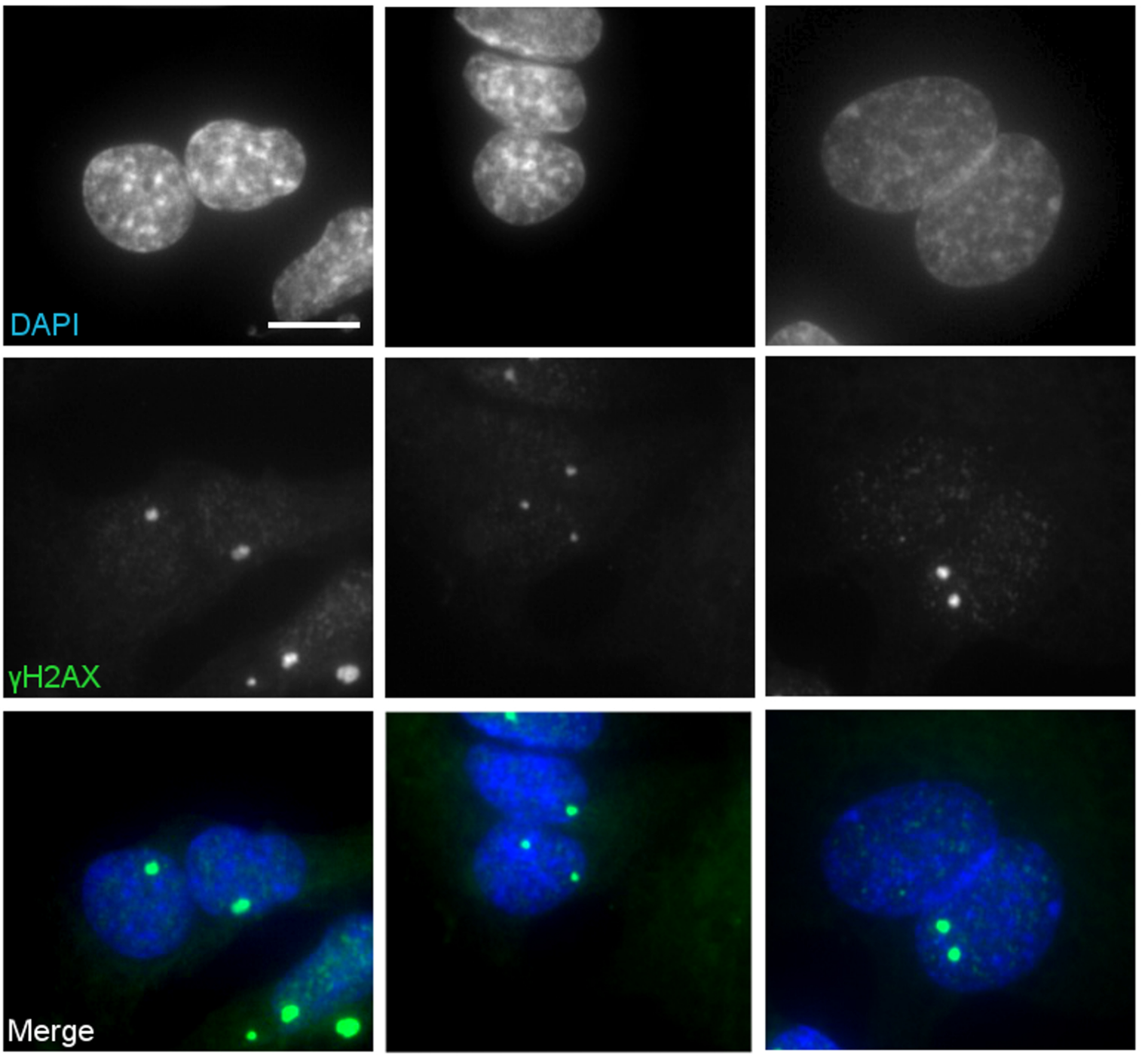

55.3% ± 3.2%	38.0% ± 2.0%	6.7% ± 2.9%
same number of persistent IRIF in both nuclei	difference of 1 persistent IRIF in both nuclei	difference of 2 persistent IRIF in both nuclei

Fig. 8

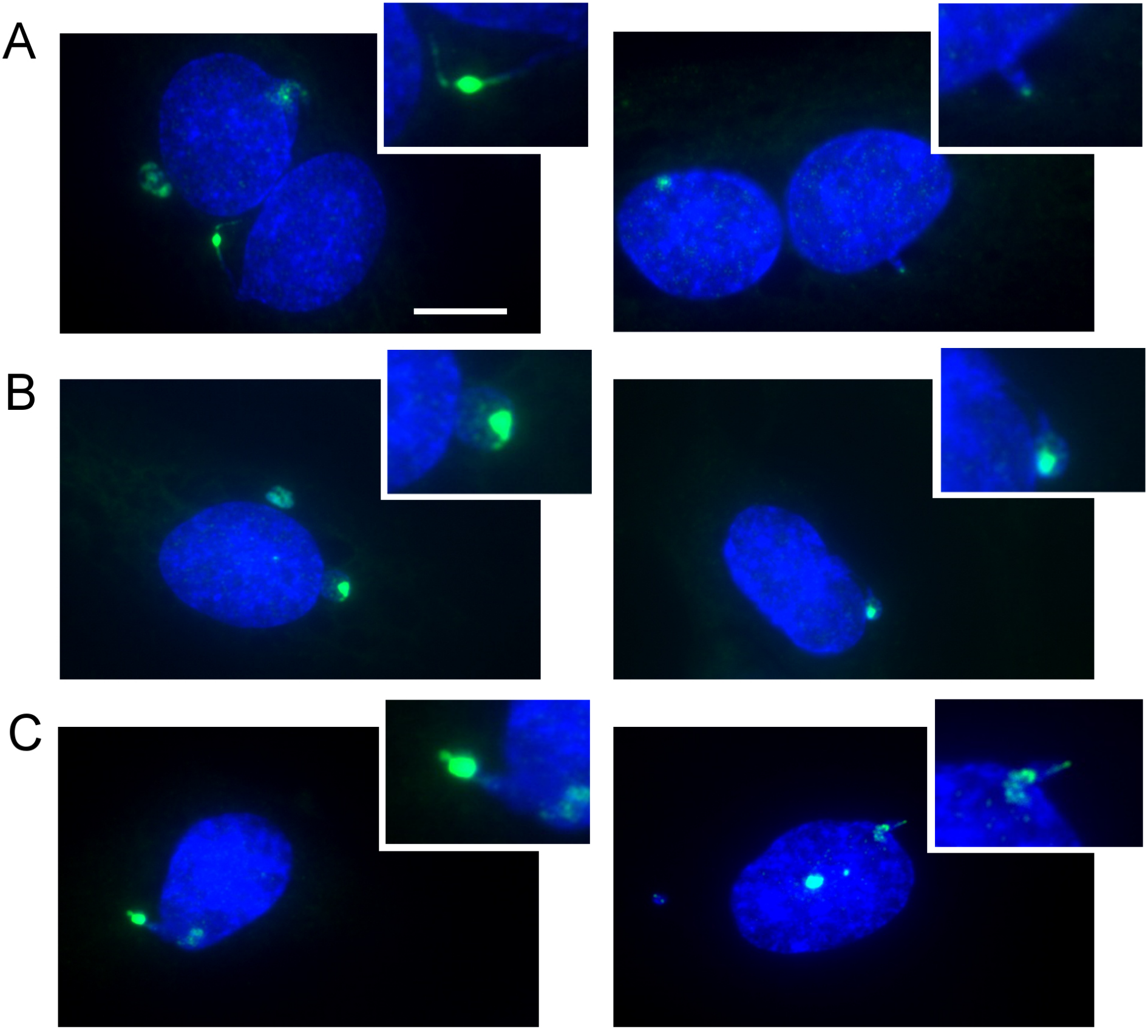

Fig. 9

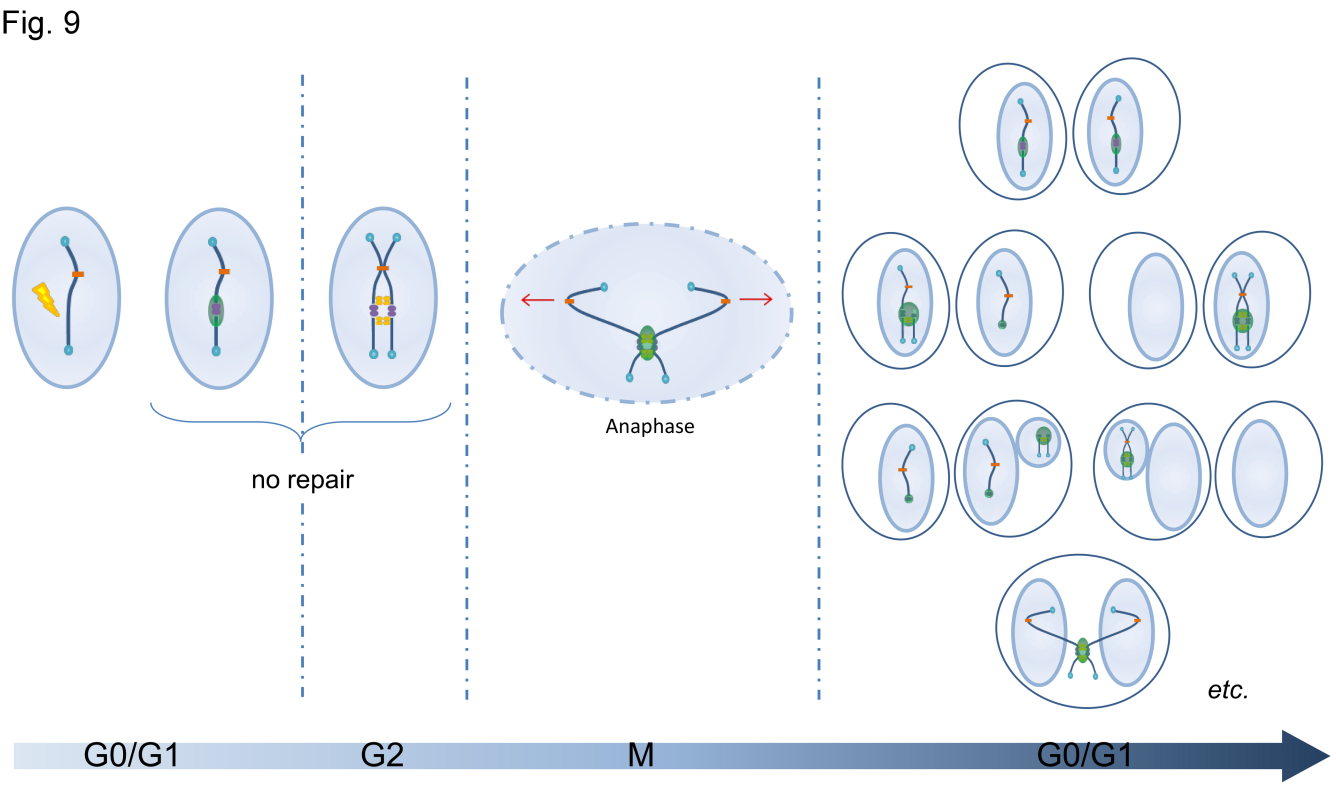

Table 1. Frequency of γH2AX foci in G0/G1 cells exposed to X-rays

	Radiation dose	Time after exposure				
		24h	48h	72h	96h	168h
Frequency of γH2AX foci per cell [a]	0Gy	0.27	0.22	0.26	0.25	0.39
	1Gy	0.86**	0.48***	0.45	0.52	0.59
	5Gy	4.22***	2.23***	1.67***	1.33**	0.84*
Frequency of large γH2AX foci per cell [a]	0Gy	0.05	0.05	0.05	0.05	0.05
	1Gy	0.23*	0.19**	0.16**	0.13**	0.10
	5Gy	2.02**	1.34***	1.19***	0.97***	0.53**

[a] Values represent means calculated on five experiments (about 1 300 to 11 000 cells by condition)

Value significantly different of unirradiated cells using Student T-test with:

* $\alpha < 0.05$, or ** $\alpha < 0.01$, or *** $\alpha < 0.001$

Table 2. Frequency of cells with micronuclei and/or nucleoplasmic bridges in G0/G1 BrdU-positive cells

Radiation dose	All cells [a]	Cells with γH2AX signal [a, b]	Cells without γH2AX signal [a]
0Gy	9.1% ± 1.0%	59.6% ± 17.8%	40.4% ± 17.8%
1Gy	23.4% ± 3.6%	85.7% ± 0.8%	14.3% ± 0.8%
5Gy	78.0% ± 4.5%	86.5% ± 1.4%	13.5% ± 1.4%

[a] Values represent means and s.e. calculated on three experiments (around 700 cells by condition)

[b] Corresponding to γH2AX signal observed in nuclei, micronuclei or nucleoplasmic bridges